FREQUENCY-MODULATED CONTINUOUS-WAVE RADAR PROCESSING FUNDAMENTALS

BY

KIRK BUSCHE

THESIS

Submitted in partial fulfillment of the requirements
for the degree of Master of Science in Electrical and Computer Engineering
in the Graduate College of the
University of Illinois at Urbana-Champaign, 2019

Urbana, Illinois

Adviser:

Professor Minh Do

ABSTRACT

In this thesis, we will discuss the techniques for determining distances, velocities, and angular position of targets using a frequency-modulated continuous-wave (FMCW) radar. FMCW radars have applications such as collision detection and assisted cruise control in modern vehicles, due to their ability to be manufactured as low-power, single-chip systems. We will discuss the use of a two-dimensional fast Fourier transform to efficiently compute the Doppler-range bins for a linear FMCW. A rudimentary geometric approach to angle estimation will then be discussed, followed by a look at the multiple signal classification (MUSIC) approach for angle estimation. Finally, we present the results of a simulated FMCW radar system with ideal targets for a variety of configurable system parameters.

In memory of my mother.

ACKNOWLEDGMENTS

I would like to thank my adviser, Prof. Minh Do, for his guidance and support throughout the research process, in addition to chatting about our shared passion for distance running. I also would like to thank the members of the Computational Imaging Group for their support and friendship. Finally, I would like to thank my family and friends for their ongoing love and support.

TABLE OF CONTENTS

LIST OF FIGURES

CHAPTER 1

INTRODUCTION

Traditionally, radar systems consisted of discrete components with high system cost and power consumption, but the recent development of integrated single-chip frequency-modulated continuous-wave (FMCW) radars has significantly reduced the cost, size, and power consumption of these systems. These integrated CMOS FMCW radar systems operate at 76-81 GHz, with radial range resolutions as high as 3.75 cm due to sweep bandwidths up to 4 GHz and velocity resolutions as high as 0.05 m/s. Due to regulations and available bandwidths, previous radar systems operating at lower frequencies (< 24 GHz) have smaller sweep bandwidths, leading to reduced range resolutions and reduced velocity resolutions, due to the larger carrier wavelengths. Given these recent developments in high-frequency, wide-band radar, we predict that these radar devices will revolutionize wireless sensing and imaging capabilities.

Modern vehicles are equipped with a wide variety of available data, including vehicle odometry, and in recent years cars have been equipped with cameras and radar for features like collision detection and traffic-aware cruise control.

In recent years, the computer vision community has made dramatic progress on classification, detection, tracking, and other problems with the development of deep neural networks, using large labeled training datasets. However, vision alone cannot solve certain problems such as position and velocity measurements with satisfactory results, but radar systems excel at these. Additionally, environmental conditions such as rain, fog, smoke, and dust significantly hinder visible system performance, but radar performance is relatively unaffected in these situations [1].

In this thesis, we will cover the mathematics for determining range and velocity, and for estimating angle of arrival, for targets in front of an FMCW radar.

CHAPTER 2

ESTIMATING RANGE

As the name frequency-modulated continuous-wave (FMCW) implies, an FMCW radar is a continuous time system which transmits and receives a periodic signal whose frequency has been modulated. As a periodic signal, the transmitted signal has the complex form (with unit-normalized amplitude)

$$p(t) = e^{j2\pi f(t)t}. \tag{2.1}$$

The typical frequency modulation used in FMCW radar systems is the sawtooth modulation, given by [2, 3]

$$f(t) = f_c + \alpha(t - kT_c), \quad \text{for } kT_c \leq t < (k+1)T_c, \quad k \in \mathbb{Z}, \tag{2.2}$$

where $\alpha > 0$ is the chirp-rate $\frac{df}{dt}$, f_c is the base carrier frequency (e.g. 77 GHz), and T_c is the period of the chirp, as shown in Figure 2.1.

To simplify the calculations, we will deal with a single chirp for range calculations, thus the frequency for a single chirp is

$$f(t) = f_c + \alpha t \quad \text{for } 0 \leq t < T_c. \tag{2.3}$$

The maximum frequency of each chirp is

$$f_{max} \triangleq f_c + \alpha T_c, \tag{2.4}$$

and the bandwidth B of the signal is

$$B = f_{max} - f_c = \alpha T_c. \tag{2.5}$$

Combining the sawtooth frequency modulation (2.2) with the complex

sinusoid (2.1), we get the transmitted (TX) signal as

$$p(t) = e^{j(2\pi f_c t + \pi \alpha t^2)}. \tag{2.6}$$

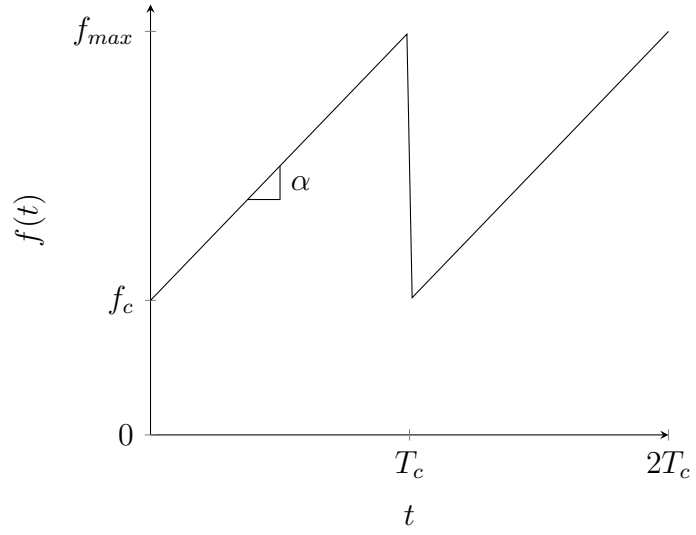

(a) Example of sawtooth frequency modulation

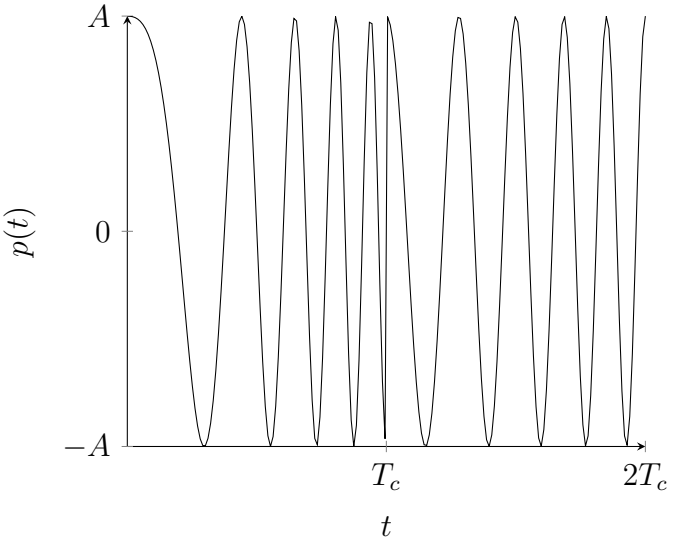

(b) Example of TX signal $p(t)$

Figure 2.1: Sawtooth frequency modulation and corresponding transmitted signal

Consider a target at a distance d from the radar, such that the transmitted (RX) signal reflects off the target and returns to the radar. This received signal will be a time-delayed version of the TX signal, where the time delay

τ is given by

$$\tau = \frac{2d}{c}, \tag{2.7}$$

where c is the speed of light. The RX signal thus has the form

$$p(t-\tau) = e^{j(2\pi f_c(t-\tau)+\pi\alpha(t-\tau)^2)}. \tag{2.8}$$

Figure 2.2 depicts the effect of τ on the sawtooth frequency modulation.

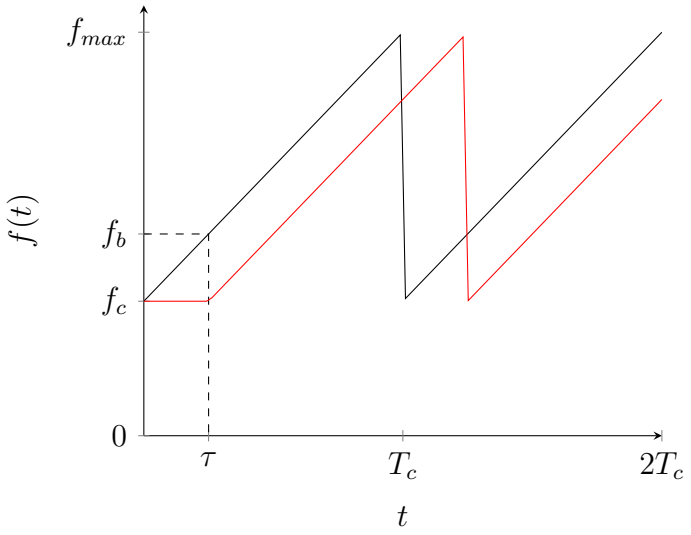

Figure 2.2: Frequency of RX signal (delayed by time τ)

To recover τ, and subsequently d, we define a new dechirped signal $r(t)$ as the product of the transmitted signal with the complex conjugate of the received signal

$$\begin{aligned} r(t) &\triangleq p(t)p^*(t-\tau) && (2.9)\\ &= e^{j(2\pi f_c t+\pi\alpha t^2)}e^{-j[2\pi f_c(t-\tau)+\pi\alpha(t-\tau)^2]} && (2.10)\\ &= e^{j(2\pi f_c\tau-\pi\alpha\tau^2)}e^{j2\pi\alpha\tau t}. && (2.11) \end{aligned}$$

Note that the first exponential in (2.11) only depends on τ, so it is a constant phase term. However, the second term varies according to a constant frequency (named the beat frequency) f_b

$$f_b \triangleq \alpha\tau. \tag{2.12}$$

Recovering f_b allows us to recover the distance d as

$$d = \frac{cf_b}{2\alpha}. \tag{2.13}$$

The maximum beat frequency occurs when $\tau = T_c$, as any $\tau \in (T_c, 2T_c]$ will appear as τ^*

$$\tau^* = \tau - T_c, \quad \tau \in (T_c, 2T_c], \tag{2.14}$$

and thus the recovered distance d^* will be less than the true range of the target from the radar. From this, we can get our maximum recoverable distance for a given chirp period

$$d_{max} = \frac{cT_c}{2}. \tag{2.15}$$

To recover the beat frequency f_b from the dechirped signal, $r(t)$, we can simply use the Fourier transform to get

$$\begin{aligned} R_r(f) &= \int_{-\infty}^{\infty} r(t) e^{-j2\pi ft} dt && (2.16)\\ &= \int_{-\infty}^{\infty} e^{j(2\pi f_c \tau - \pi\alpha\tau^2)} e^{j2\pi\alpha\tau t} e^{-j2\pi ft} dt && (2.17)\\ &= e^{j(2\pi f_c \tau - \pi\alpha\tau^2)} \int_{-\infty}^{\infty} e^{-j2\pi(f-\alpha\tau)t} dt && (2.18)\\ &= e^{j(2\pi f_c \tau - \pi\alpha\tau^2)} \delta(f - \alpha\tau), && (2.19) \end{aligned}$$

where $\delta(f)$ is the Dirac delta function.

Now consider the case of multiple (N) objects at different distances d_i from the radar

$$d_i \neq d_j \quad \text{for } i \neq j, \quad i, j \in [1, N]. \tag{2.20}$$

Each of these objects will reflect the transmitted chirp with a unique delay τ_i, as seen in Figure 2.3, and therefore will have a unique beat frequency corresponding to these delays. Using the continuous-time Fourier transform, we can always resolve the unique beat frequencies corresponding to the time delays.

However, in practice we must sample the received signal $r(t)$ with an analog-to-digital converter (ADC), with sampling frequency $f_s = 1/T_s$. To retrieve the beat frequencies, we take the M-point discrete Fourier transform

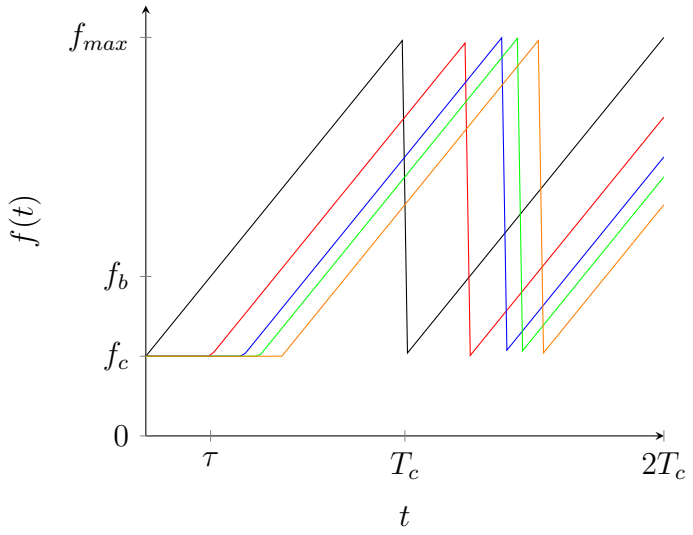

Figure 2.3: Frequencies of reflected signals from multiple objects

(DFT) [4] of $r(t)$ for each chirp period

$$R_r[f] = \sum_{m=0}^{M-1} r[mT_s] e^{-j\frac{2\pi}{M}fm} \tag{2.21}$$

$$= \sum_{m=0}^{M-1} e^{j(2\pi f_c \tau - \pi\alpha\tau^2)} e^{j2\pi\alpha\tau m T_s} e^{-j\frac{2\pi}{M}fm}. \tag{2.22}$$

From this, we can see that $R_r[f]$ has a peak when $f = MT_s\alpha\tau$, and since M, T_s, and α are configured parameters, we can recover τ and subsequently the distance d. This processing can be done efficiently on hardware with the fast Fourier transform (FFT), so this step is often called the range-FFT.

Since we are using the DFT, we can only resolve frequency components separated by $1/T_{window}$, where T_{window} is the observation window,

$$\Delta f > \frac{1}{T_{window}}. \tag{2.23}$$

Now let the observation window be the chirp period, T_c, such that, from (2.13), we get the range-cell resolution

$$\Delta d = \frac{c\Delta f}{2\alpha} \tag{2.24}$$

$$\implies \Delta d > \frac{c}{2\alpha T_c} = \frac{c}{2B}. \tag{2.25}$$

With an M-point DFT, the maximum recoverable frequency is

$$f_{b,max} = \frac{M-1}{T_s M}, \tag{2.26}$$

so the maximum recoverable distance is

$$d_{max} = \frac{(M-1)c}{2\alpha T_s M}. \tag{2.27}$$

CHAPTER 3

ESTIMATING VELOCITIES

To determine the velocity of an object, we can compare the phases of two chirps reflected from the moving object. Recall from (2.11) that the first exponential term in $r(t)$ has no dependence on t, so it fully describes the phase. We can approximate this phase as a linear function of the time delay τ,

$$\phi(r(t)) = 2\pi f_c \tau - \pi\alpha\tau^2 + 2\pi\alpha\tau t \tag{3.1}$$

$$\implies \angle r(t) \approx 2\pi f_c \tau. \tag{3.2}$$

For an object moving with velocity v and initial range d_0, the time delay τ is given by

$$\tau = \frac{2(d_0 + vt)}{c}, \tag{3.3}$$

so the linear phase approximation becomes

$$\phi(r(t)) \approx \frac{4\pi(d_0 + vt)}{\lambda}, \tag{3.4}$$

where $\lambda = \frac{c}{f_c}$ the wavelength of the carrier signal. Now, the phase difference $\Delta\phi$ between two dechirped signals separated by T_c is

$$\Delta\phi = \frac{4\pi\Delta d}{\lambda}, \tag{3.5}$$

where Δd is the distance the object travels over T_c between the two chirps. For an object traveling at a velocity v, this distance is

$$\Delta d = vT_c, \tag{3.6}$$

so the phase difference becomes

$$\Delta\phi = \frac{4\pi v T_c}{\lambda}. \tag{3.7}$$

However, phase difference is inherently ambiguous unless $|\Delta\phi| < \pi$, so we find that the maximum velocity measurable by two chirps spaced T_c apart is given by

$$v_{max} = \frac{\lambda}{4T_c}. \tag{3.8}$$

This two-chirp approach fails if we have multiple objects moving with different velocities, but the same range, at the time of measurement. The reflected chirps will produce identical beat frequencies in this scenario, so the range processing Fourier transform will result in a single peak representing the combined signals from the equidistant objects. In this case, we can use K equally spaced chirps transmitted by the radar over a chirp frame $T_f = KT_c$, as shown in Figure 3.1.

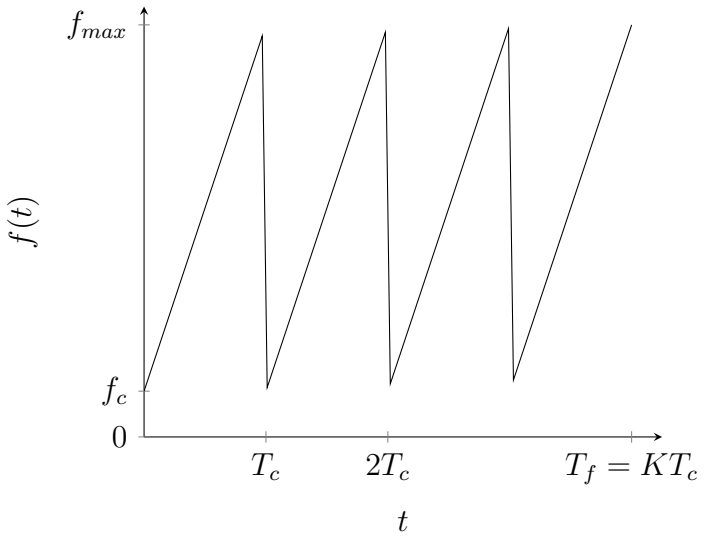

Figure 3.1: Chirp frame T_f consisting of K chirps

Now we will need to use the full sawtooth frequency modulation as described in (2.2), so $p(t)$ is

$$p(t) = e^{j(2\pi f_c t + \pi\alpha t^2 - 2\pi\alpha k T_c t)}. \tag{3.9}$$

Then, the dechirped signal $r(t)$ will be

$$r(t) = e^{j(2\pi f_c \tau - \pi\alpha\tau^2 + 2\pi\alpha\tau(t-kT_c))}. \tag{3.10}$$

Again, we approximate by eliminating the quadratic components to get

$$\phi(r(t)) \approx 2\pi(f_c + \alpha t_k)\tau, \tag{3.11}$$

where

$$t_k \triangleq t - kT_c \quad \text{for } k \in \mathbb{Z}. \tag{3.12}$$

Substituting (3.3) into (3.11) gives

$$\begin{aligned}
\phi(r(t)) &\approx \frac{4\pi}{c}(f_c d_0 + f_c v t + \alpha d_0 t_k) && (3.13)\\
&= 2\pi(f_c\tau_0 + f_d t + t_k f_\tau) && (3.14)\\
&= 2\pi(f_c\tau_0 + f_d k T_c + (f_\tau + f_d)t_k), && (3.15)
\end{aligned}$$

where τ_0 is the initial time delay, f_d is the Doppler frequency, and f_τ is the range-beat-frequency, as defined below.

$$\begin{aligned}
\tau_0 &\triangleq \frac{2d_0}{c} && (3.16)\\
f_d &\triangleq \frac{2v}{c} f_c && (3.17)\\
f_\tau &\triangleq \alpha\tau_0. && (3.18)
\end{aligned}$$

For each k-th chirp, we compute $R_r(f,k)$ as in (2.16), which contains the range information for the objects,

$$\begin{aligned}
R_r(f,k) &= \int_\tau^{T_c} r(t_k) e^{-j2\pi f t_k} dt_k && (3.19)\\
&= \int_\tau^{T_c} e^{j\phi(r(t_k))} e^{-j2\pi f t_k} dt_k && (3.20)\\
&= \int_\tau^{T_c} e^{j2\pi(f_c\tau_0 + f_d k T_c + (f_\tau + f_d)t_k)} e^{-j2\pi f t_k} dt_k. && (3.21)
\end{aligned}$$

The absolute value $|R_r(f,k)|$ is obtained for $f = f_d + f_\tau$, and, in general, $f_\tau >> f_d$, so we can resolve the ranges as before. Now, since the term $f_d k T_c$ depends on k, we see that $R_r(f,k)$ is a function of k, with sampling

period T_c, observed K consecutive times over the course of the chirp frame T_f. Each of these k spectra will have a different phase which combines the phase contributions from each object at the corresponding range with different velocities. This spectrum is described by the following DFT:

$$R(f,n) = \sum_{k=0}^{K-1} R_r(f,k) e^{-j\frac{2\pi}{K}kn}, \tag{3.22}$$

which achieves maximum absolute value (i.e. a peak) when

$$n = f_d T_c. \tag{3.23}$$

In the case of multiple objects at the same range, but with different velocities, we will have peaks corresponding to the Doppler frequencies of each object, enabling us to resolve the different velocities. Since we are using the DFT, we can derive the velocity resolution as we did the range resolution in (2.25), where the observation window here is the frame time T_f,

$$\Delta v = \frac{c}{2KT_c f_c} = \frac{c}{2f_c T_f}. \tag{3.24}$$

This spectrum is computed using the FFT method, so we call this step the Doppler-FFT. By reordering the samples of $r(t)$ into a 2D matrix $\boldsymbol{R}$ where each row is the samples from one chirp period T_c with K rows (i.e. K chirps), we can compute the range-FFT and Doppler-FFT as a 2D FFT over the data matrix $\boldsymbol{R}$.

CHAPTER 4

COMPUTING ANGLE OF ARRIVAL

If the radar has at least two transmit-receive antenna pairs, we can calculate the angle of arrival (AoA) for the received signal from the phase differences in the spectra, which arise from the slight differences in range of the object from each receiving antenna.

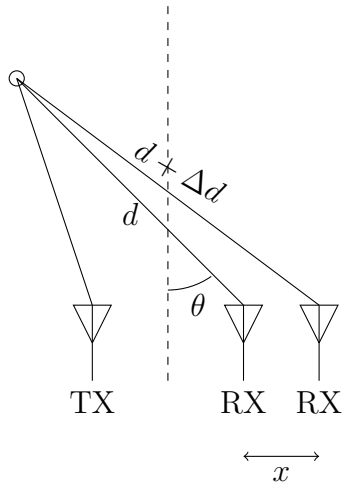

Figure 4.1: Angle of arrival problem

4.1 Geometric Estimation

From Figure 4.1, we can derive the phase difference between the received signals $r_1(t)$ and $r_2(t)$ at two different antennas separated by a distance x. Let d be the distance the received signal $r_1(t)$ travels to reach the first antenna and $d + \Delta d$ be the distance the reflected signal $r_2(t)$ travels to reach the second antenna [5]. Assuming the radar signal is a planar wavefront, the geometry shown in Figure 4.2 gives

$$\Delta d = x \sin \theta. \tag{4.1}$$

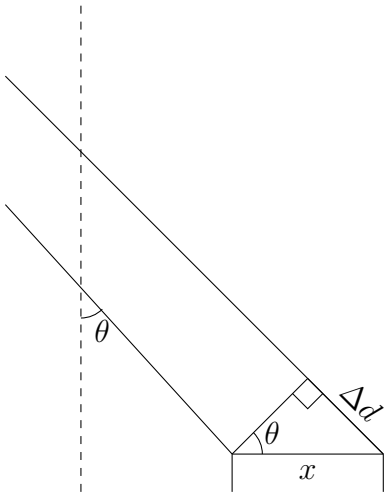

Figure 4.2: Geometric approach for estimating angle of arrival

Now, the phase difference $\Delta\phi$ is given by

$$\Delta\phi = \frac{2\pi\Delta d}{\lambda}. \tag{4.2}$$

Now, we can compute the angle of arrival θ as

$$\theta = \sin^{-1}(\frac{\lambda\Delta\phi}{2\pi x}). \tag{4.3}$$

However, since $\Delta\phi$ depends on $\sin\theta$, our accuracy degrades for large θ, as $\sin\theta \approx \theta$ only for small θ.

As before, for the phase difference to be unambiguous, $|\Delta\phi| < \pi$, so we find

$$\frac{2\pi x}{\lambda}\sin\theta < \pi, \tag{4.4}$$

and the maximum field of view for two TX-RX antenna pairs spaced x apart is

$$\theta_{max} = \sin^{-1}(\frac{\lambda}{2x}). \tag{4.5}$$

Clearly, the largest angular field of view for two antenna pairs with this approach occurs when the antenna spacing is

$$x = \frac{\lambda}{2}, \tag{4.6}$$

giving $\theta_{max} = \pm\frac{\pi}{2}$.

4.2 Multiple Signal Classification (MUSIC)

For multiple-input multiple-output (MIMO) FMCW radar systems, we can use more sophisticated angle-of-arrival techniques based on subspaces. Let us assume we have an arbitrary array of L virtual transmit-receive antenna pairs, with an array response vector $\boldsymbol{a}(\theta)$. This response vector maps the direction of arrival θ to the signal phase shift at each of the L virtual antenna pairs. For a set of N objects, we will have N return signals $r(t)$ returning to the antenna array. Let $\boldsymbol{x}(t)$ be the superposition of the signals so that [6]

$$\boldsymbol{x}(t) = \sum_{n=1}^{N} s_n(t)\boldsymbol{a}(\theta_n) \tag{4.7}$$

$$= \boldsymbol{A}(\boldsymbol{\theta})\boldsymbol{s}(t), \tag{4.8}$$

where

$$\boldsymbol{A}(\boldsymbol{\theta}) = [\boldsymbol{a}(\theta_1), \boldsymbol{a}(\theta_2), \ldots, \boldsymbol{a}(\theta_N)] \tag{4.9}$$

$$\boldsymbol{\theta} = [\theta_1, \theta_2, \ldots, \theta_N]^T \tag{4.10}$$

$$\boldsymbol{s}(t) = [s_1(t), s_2(t), \ldots, s_N(t)]^T. \tag{4.11}$$

If we sample $\boldsymbol{x}(t)$ at M timesteps, we get the following matrix equation:

$$\boldsymbol{X} = \boldsymbol{A}(\boldsymbol{\theta})\boldsymbol{S}, \tag{4.12}$$

where $\boldsymbol{X}$ is an $L \times M$ matrix of samples, $\boldsymbol{A}(\boldsymbol{\theta})$ is an $L \times N$ matrix function, and $\boldsymbol{S}$ is a $N \times M$ matrix

$$\boldsymbol{X} = [\boldsymbol{x}(t_1), \boldsymbol{x}(t_2), \ldots, \boldsymbol{x}(t_M)] \tag{4.13}$$

$$\boldsymbol{S} = [\boldsymbol{s}(t_1), \boldsymbol{s}(t_2), \ldots, \boldsymbol{s}(t_M)]. \tag{4.14}$$

Since $\boldsymbol{X}$ is the product of an $L \times N$ matrix and an $N \times M$ matrix, we have that $rank(\boldsymbol{X}) = N$, assuming $\boldsymbol{A}(\boldsymbol{\theta})$ has full column rank and $\boldsymbol{S}$ has full row rank. This corresponds to the number of objects whose angular position we are trying to compute. Now, since the range space of $\boldsymbol{X}$, $\mathcal{R}(\boldsymbol{X})$, is the same subspace as the range space of $\boldsymbol{A}(\boldsymbol{\theta})$

$$\mathcal{R}(\boldsymbol{X}) = \mathcal{R}(\boldsymbol{A}(\boldsymbol{\theta})), \tag{4.15}$$

we can use the singular value decomposition (SVD) of $\boldsymbol{X}$ to recover θ_i. The SVD of $\boldsymbol{X}$ is given by

$$\boldsymbol{X} = \boldsymbol{U}\boldsymbol{\Sigma}\boldsymbol{V}^H \tag{4.16}$$

$$= [\boldsymbol{U_s}|\boldsymbol{U_n}] \begin{bmatrix} \Sigma_s & 0 \\ 0 & \boldsymbol{0} \end{bmatrix} \boldsymbol{V}^H, \tag{4.17}$$

where the left singular vectors have been separated into those corresponding to the nonzero singular values ($\boldsymbol{U}_s$) and those corresponding to the zero singular values ($\boldsymbol{U}_n$). From linear algebra, we know the columns of $\boldsymbol{U}_s$ span the signal subspace $\mathcal{R}(\boldsymbol{X})$ and the columns of $\boldsymbol{U}_n$ span the left nullspace $\mathcal{N}\boldsymbol{X}^H$) of $\boldsymbol{X}$, which is the orthogonal complement of the signal subspace [7]. In this context, we will call this subspace the noise subspace

$$\text{span}(\boldsymbol{U_n}) = \mathcal{N}(\boldsymbol{X}^H) \tag{4.18}$$

$$= \mathcal{R}(\boldsymbol{X})^{\perp} \tag{4.19}$$

$$= \mathcal{R}(\boldsymbol{A}(\boldsymbol{\theta}))^{\perp}. \tag{4.20}$$

Now, if we sweep $\theta \in [0, 2\pi)$, $\boldsymbol{a}(\theta)$ will lie in the left nullspace of $\boldsymbol{X}$ when $\theta = \theta_i$, where θ_i are the desired angles of arrival we are estimating,

$$\theta = \theta_i \iff \boldsymbol{U}_n^H \boldsymbol{a}(\theta) = 0. \tag{4.21}$$

The multiple signal classification (MUSIC) algorithm leverages this fact by finding the peaks in [8]

$$g(\theta) = \frac{1}{\|\boldsymbol{U}_n^H \boldsymbol{a}(\theta)\|^2}. \tag{4.22}$$

CHAPTER 5

EXPERIMENTS

Recall that an FMCW radar system has several configurable parameters, including the chirp rate α, the chirp period T_c, and the number of chirps K in a chirp frame. To verify the FMCW radar mathematics and investigate the effects of these parameters, we ran several simulations in Python.

For these simulations we modeled the radar system after Texas Instruments's IWR 1443 FMCW chip, which has a carrier frequency f_c of 77 GHz and a sampling frequency of 3 Msps [9]. We will use a 256-point FFT for the range-FFT and a 32-point FFT for the Doppler-FFT. For these simulations, we are just investigating the range-FFT and Doppler-FFT behavior, so we simplify the model to have a single transmit-receive antenna pair. Additionally, we will assume we have ideal point targets with no attenuation to better isolate the effects of the system parameters within the simulations. We will simulate three targets with different ranges and velocities, as shown in Table 5.1. For this model, we also include additive white Gaussian noise on the received signal.

Table 5.1: Simulated target initial positions and velocities

Target	Range	Velocity
Target 1	5.0 m	0 m/s
Target 2	10.0 m	5.0 m/s
Target 3	20.0 m	-7.5 m/s

We will consider a baseline case with a chirp period of 60 μs, a bandwidth of 500 MHz, 30 chirps per chirp frame, a 256-point range-FFT, and a 32-point Doppler-FFT. As the bandwidth, chirp period, and chirp rate are intrinsically linked, we only need to define two parameters to determine all three. These parameters give a range resolution of 21.1 cm, a maximum distance of 53.79 m, a velocity resolution of 1.01 m/s, and a velocity range of $\pm$15.2 m/s. Figure 5.1 shows the range-FFT for a single chirp and the range-Doppler

plot for this parameter selection. We can clearly see three peaks in both plots, corresponding to the three targets. The recovered distances were 5.06 m, 10.13 m, and 19.83 m. Likewise, the recovered velocities were 0.0 m/s, 5.07 m/s, and -7.10 m/s.

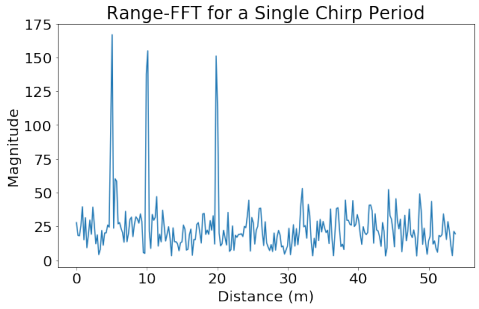

(a) Range-FFT for a single chirp with the baseline parameters

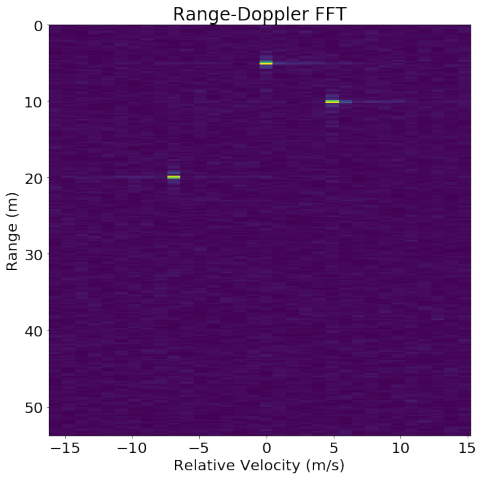

(b) Doppler-FFT for the baseline parameters

Figure 5.1: Baseline simulation results

Now consider the case where the bandwidth is doubled to 1 GHz while maintaining the same chirp period. This clearly doubles the chirp rate, giving us a range resolution of 10.5 cm, but a maximum distance of only 26.9 m, keeping the other parameters the same from the baseline simulation. We can see from the results shown in Figure 5.2 that we still have three clear peaks corresponding to the targets, with recovered distances 4.96 m, 10.02 m, and 19.93 m and corresponding recovered velocities of 0.0 m/s, 5.07 m/s, and -7.10 m/s. Though both plots show the improved range resolution, the range-Doppler plot more clearly shows the range resolution change as the pixel widths corresponding to the range bins are more clearly demarcated.

To see the effect of the chirp period, let us examine the baseline system with the chirp period doubled to 120 μs. With a bandwidth of 500 MHz, this halves the chirp rate of the baseline system. By halving the chirp rate, our range resolution decreases to 42.2 cm and the maximum range increases to 107.6 m. We also see the velocity resolution improve to 0.51 m/s but the velocity range is halved to $\pm$7.61 m/s. Figure 5.3 shows the simulation results, with recovered distances 5.06 m, 10.13 m, and 19.83 m. We see that

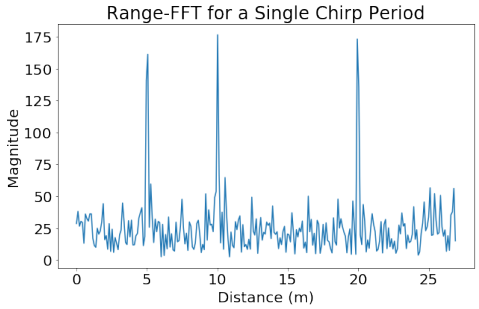

(a) Range-FFT for a single chirp with 1 GHz bandwidth

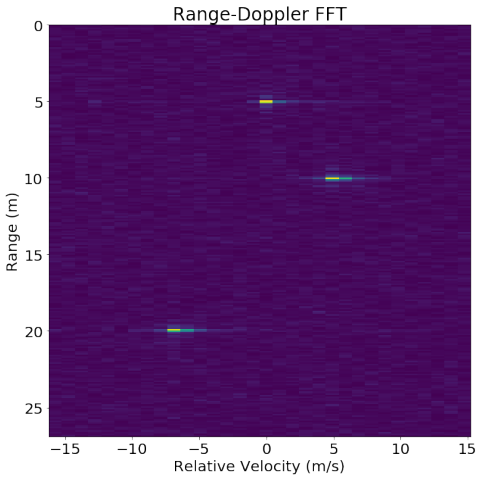

(b) Doppler-FFT for the 1 GHz bandwidth version of the baseline system

Figure 5.2: Increased bandwidth simulation results

the Doppler-FFT recovers two clean peaks for the first two targets, with recovered velocities 0.0 m/s and 5.07 m/s respectively. However, due to the FFT smearing, the second target's velocity of -7.5 m/s is split between two peaks recovered at -7.61 m/s and -7.1 m/s.

Now, if we replicate the baseline system, except with a chirp frame of only 15 chirps, we expect to only see a difference in the Doppler results. In fact, we can clearly see the sinc function in the Doppler-FFT in Figure 5.4, as we are padding the input signal of length 15 (number of chirps) to be length 32 for the FFT. This increase in zero-padding from the baseline case more clearly shows the Doppler-FFT sampling on the non-zero points of the rectangle window spectrum, causing this spectrum leakage. Choosing a different windowing function, such as the Hamming window, could help alleviate this spectral leakage, though more investigation into the proper window choice is still required.

Table 5.2 provides a summary of the different scenarios simulated here.

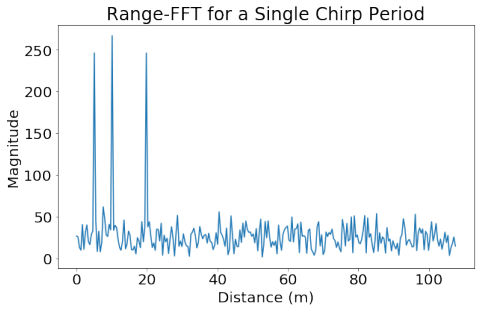

(a) Range-FFT for a single chirp with period 120 μs

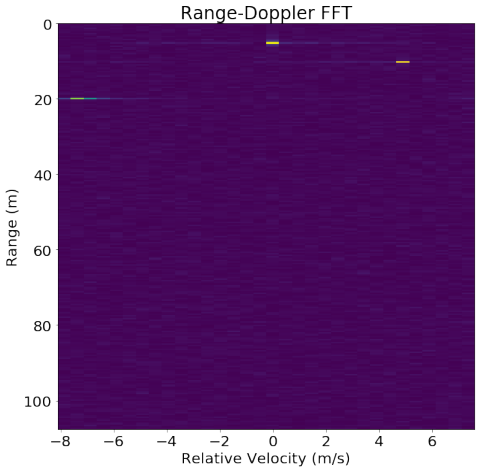

(b) Doppler-FFT for 120 μs chirp period system

Figure 5.3: Increased chirp period simulation results

Table 5.2: List of simulation parameters

Simulation	Bandwidth	Chirp Period	Chirp Rate	Number of Chirps
Baseline	500 MHz	60 μs	8.33 MHz/μs	30
Bandwidth	**1 GHz**	60 μs	**16.67 MHz/μs**	30
Chirp Period	500 MHz	**120 μs**	**4.167 MHz/μs**	30
Chirp Number	500 MHz	60 μs	8.33 MHz/μs	**15**

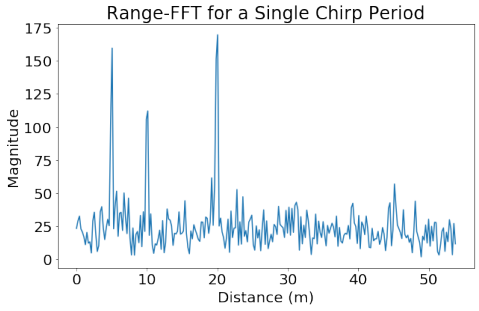

(a) Range-FFT for a single chirp

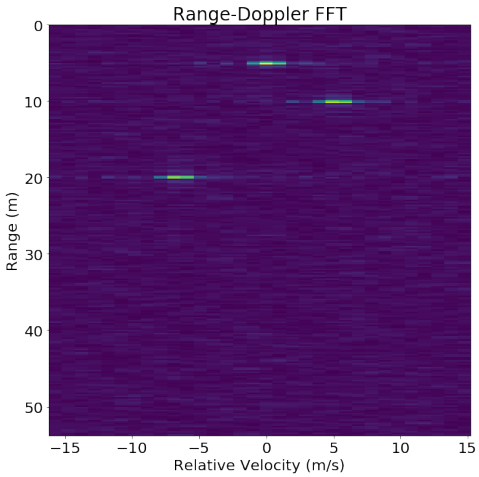

(b) Doppler-FFT for 15 chirps/frame system

Figure 5.4: Decreased number of chirps per frame results

CHAPTER 6

CONCLUSION

In this work, the processing chain for linear frequency-modulated continuous-wave radars was explored. We demonstrated how the sawtooth frequency modulation gives rise to the beat-frequency phenomenon from the combined transmit-receive signals and contains the range information via the time delay. Furthermore, we investigated the influence of an object's velocity on the phases for return signals corresponding to different chirps and how to leverage this information with a second Fourier transform to recover the Doppler frequencies. Next, we discussed angular position estimation for multiple-input multiple-output radar systems, first by a simple geometric estimation and second by the subspace-based multiple signal classification (MUSIC) algorithm. Finally, we presented simulated results of a 77 GHz FMCW radar system based on Texas Instruments's IWR 1443 chip and investigated the effects of several configurable system parameters on range and velocity detection performance.

REFERENCES

[1] V. M. Patel, J. N. Mait, D. W. Prather, and A. S. Hedden, "Computational millimeter wave imaging: Problems, progress, and prospects," *IEEE Signal Processing Magazine*, vol. 33, no. 5, pp. 109–118, 2016.

[2] A. G. Stove, "Linear FMCW radar techniques," in *IEE Proceedings F (Radar and Signal Processing)*, vol. 139, no. 5. IET, 1992, pp. 343–350.

[3] B.-C. Wang, *Digital Signal Processing Techniques and Applications in Radar Image Processing*. John Wiley & Sons, 2008, vol. 91.

[4] M. Vetterli, J. Kovačević, and V. K. Goyal, *Foundations of Signal Processing*. Cambridge University Press, 2014.

[5] C. Iovescu and S. Rao, "The fundamentals of millimeter wave sensors," *Texas Instruments, SPYY005*, 2017.

[6] Y. Bresler, S. Basu, and C. Couvreur, "Hilbert spaces and least squares methods for signal processing," 2017, unpublished, University of Illinois Urbana-Champaign.

[7] C. D. Meyer, *Matrix Analysis and Applied Linear Algebra*. SIAM, 2000.

[8] R. Schmidt, "Multiple emitter location and signal parameter estimation," *IEEE Transactions on Antennas and Propagation*, vol. 34, no. 3, pp. 276–280, 1986.

[9] "IWR 1443 data sheet," Texas Instruments, Dallas, Texas.